Numerical homogenisation of micromorphic media

R. Jänicke, S. Diebels

Due to their underlying microtopology, cellular materials are known to show a complex mechanical behaviour. For the material modelling, the heterogeneous microcontinuum is commonly replaced by a homogeneous macrocontinuum involving extended kinematics. An appropriate homogenisation methodology will be introduced in order to replace a heterogeneous Cauchy microcontinuum by a homogeneous micromorphic macrocontinuum. For an artificial 2-D periodic microstructure, the present contribution draws a comparison between extended two-scale calculations on the one hand, and a reference solution as well as a first-order FE^2 calculation on the other hand.

1 Introduction

The mechanics of cellular materials is well-known to be strongly dominated by the underlying microtopology. In literature, there exists a wide range of contributions accounting for size dependent stiff or soft boundary layer effects inducing size dependent effective material properties, cf., beyond many others, e. g. Diebels and Steeb (2002); Tekoğlu and Onck (2005). Various approaches replace the heterogeneous microcontinuum by a homogeneous macrocontinuum enriched by additional degrees of freedom. Many of those approaches go back to the seminal considerations of the brothers Cosserat and Cosserat (1909), which were later on generalised by Eringen (1999). Different approaches introduce second gradient media, e. g. Germain (1973a); Maugin (1979); Kouznetsova (2002). Otherwise, numerical methods of two-scale modelling have been developed by usage of the so-called two-level FEM or FE^2 method, e. g., beyond many others, Feyel and Chaboche (2000); Miehe and Koch (2002).

1.1 Scope of this work

In the present contribution we derive a consistent methodology to replace a heterogeneous microcontinuum of the Cauchy type, representing a cellular network, by a homogeneous micromorphic macrocontinuum. In order to bridge the scales, the extended kinematic quantities of the macroscale will be expressed in terms of a polynomial mean field and a periodic fluctuation on a microvolume attached to the macroscopic material point. Further investigations will be carried out to perform homogenisation rules for the extended macroscopic stress quantities based on an extended formulation of the Hill-Mandel condition. In sections 3 and 4, the presented methodology will be applied to a macroscopic shear test with one underlying artificial microstructure. We will restrict the extended character of the macrocontinuum as far as possible and we will verify the result in comparison to a reference calculation with microscopic resolution.

1.2 Notations

Throughout this manuscript, differential operators are defined as

$$\operatorname{div} \mathbf{T} = \frac{\partial T_{kl}}{\partial X_l}\,\mathbf{e}_k, \qquad \operatorname{GRAD} \mathbf{P} = \frac{\partial P_{kK}}{\partial X_L}\,\mathbf{e}_k \otimes \mathbf{e}_K \otimes \mathbf{e}_L,$$

where small operators and indices refer to the spatial, capital operators and indices to the material frame. Tensor products read

$$\mathbf{A} \cdot \mathbf{B} = A_{kl} B_{lm}\,\mathbf{e}_k \otimes \mathbf{e}_m, \qquad \mathbf{A} : \mathbf{B} = A_{kl} B_{kl}$$

$$\overset{3}{\mathbf{E}} \stackrel{.}{:} \mathbf{C}^{\underline{3}} = \varepsilon_{klm} C_{klm}, \qquad \mathbf{C}^{\underline{3}} \stackrel{.}{:} (\mathbf{A},\, \mathbf{B}) = C_{klm} A_{ln} B_{mo}\,\mathbf{e}_k \otimes \mathbf{e}_n \otimes \mathbf{e}_o.$$

Furthermore, the following permutation and identity tensors will be used:

$$\mathbf{I} = \delta_{kl}\mathbf{e}_k \otimes \mathbf{e}_l, \qquad \text{where} \quad \delta_{kl} = \begin{cases} 1, & k = l, \\ 0, & \text{else.} \end{cases}$$

$$\overset{3}{\mathbf{E}} = \varepsilon_{klm}\mathbf{e}_k \otimes \mathbf{e}_l \otimes \mathbf{e}_m, \qquad \text{where} \quad \varepsilon_{klm} = \begin{cases} 1, & klm = 123, \, 231, \, 312, \\ -1, & klm = 321 \, 213, \, 132, \\ 0, & \text{else.} \end{cases}$$

$$\overset{4}{\mathbf{E}} = \varepsilon_{klmn}\mathbf{e}_k \otimes \mathbf{e}_l \otimes \mathbf{e}_m \otimes \mathbf{e}_n, \quad \text{where} \quad \varepsilon_{klmn} = \begin{cases} 1, & k = l = m = n, \\ -1, & k = l \wedge m = n \wedge l \neq m \text{ and permutations,} \\ 0, & \text{else.} \end{cases}$$

Besides the permutation tensors, tensors of grade 3 and higher are denoted with underlined indices. The material time rate of a spatially represented quantity is defined as

$$(\diamond(\mathbf{x},\, t))' \quad = \quad \frac{\mathrm{d}(\diamond)}{\mathrm{d}t} \quad = \quad \frac{\partial(\diamond)}{\partial t} + \mathrm{grad}\,(\diamond) \cdot \mathbf{x}'$$

and throughout this manuscript, index $(\diamond)_M$ refers to macroscopic quantities whereas $(\diamond)_m$ refers to microscopic quantities.

2 Homogenisation of micromorphic media

2.1 The physical picture

In contrast to classical continuum theories, the micromorphic continuum theory assumes each physical body $\mathcal{B}_M$ to consist of an infinitesimal set of material points which capture a small but finite space $\mathcal{B}_m$, cf. fig. 1. Furthermore, provided the material points to be deformable, they account for additional degrees of freedom, i. e. for the microrotation and for the microdeformation, besides the classical translational degrees of freedom. This concept goes back to the brothers Cosserat and Cosserat (1909) and was later on generalised in a systematical manner e. g. by Eringen (1999).
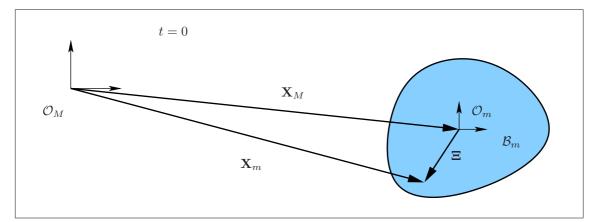

Figure 1. The material points of a micromorphic medium capture a small but finite space $\mathcal{B}_m$ and can be characterised by their volume centroid with the macroscopic position vector $\mathbf{X}_M$ and the local coordinate $\mathbf{\Xi}$ in the material frame ($t = 0$), and $\mathbf{x}_M$ and $\boldsymbol{\xi}$ in the spatial frame ($t > 0$).

The microcontinuum's mapping from the material to the spatial frame is considered to be affine and reads

$$\boldsymbol{\xi}(\mathbf{X}_M,\, \bar{\boldsymbol{\chi}}_M,\, t) \quad = \quad \bar{\boldsymbol{\chi}}_M(\mathbf{X}_M,\, t) \cdot \mathbf{\Xi}(\mathbf{X}_M), \tag{1}$$

the second order tensor $\bar{\boldsymbol{\chi}}_M$ defines the microdeformation. The calculation of the deformed arc length $(\mathrm{d}\mathbf{x}_m)^2$ requires the introduction of a set of three independent deformation measures. Without loss of generality, we establish the deformation gradient $\mathbf{F}_M$, the microdeformation $\bar{\boldsymbol{\chi}}_M$ and its first gradient $\mathrm{GRAD}\,\bar{\boldsymbol{\chi}}_M$ to describe the deformation of the physical body $\mathcal{B}_M$ on the macroscale. In spite the obviously non-objective character of this set of two-field quantities, the token choice is admissible, having in mind no macroscopic constitutive assumptions to be met throughout this contribution.

2.2 Balance equations

The balance equations for the micromorphic continuum theory can be found making use of the principle of virtual power, cf. Germain (1973b). In the sequel, the balance equations are formulated for the static and isothermal case in absence of volume forces and volume couples in the spatial and the material frame. For the balance of momentum we write

$$\operatorname{div} \mathbf{T}_M \; = \; \mathbf{0}, \qquad \operatorname{DIV} \mathbf{P}_M \; = \; \mathbf{0}, \tag{2}$$

with the Cauchy stress tensor $\mathbf{T}_M$ and the first Piola-Kirchhoff stress tensor $\mathbf{P}_M = (\det \mathbf{F}_M) \, \mathbf{T} \cdot \mathbf{F}_M^{T-1}$. The balance of moment of momentum reads

$$\operatorname{div} \breve{\mathbf{Q}}_M^3 + \mathbf{T}_M - \breve{\mathbf{S}}_M \; = \; \mathbf{0}, \qquad \operatorname{DIV} \mathbf{Q}_M^3 + (\mathbf{P}_M - \mathbf{S}_M) \cdot \mathbf{F}_M^T \; = \; \mathbf{0}, \tag{3}$$

where the third order couplestress tensor $\breve{\mathbf{Q}}_M^3$ and the second order hyperstress tensor $\breve{\mathbf{S}}_M$ of the Cauchy type have been introduced, accounting for the transformations $\mathbf{S}_M = (\det \mathbf{F}_M) \, \breve{\mathbf{S}}_M \cdot \mathbf{F}_M^{T-1}$ and $\mathbf{Q}_M^3 = (\det \mathbf{F}_M) \, \breve{\mathbf{Q}}_M^3 \cdot \mathbf{F}_M^{T-1}$. Finally, we find for the balance of energy

$$\rho \, \varepsilon_M' \; = \; \mathbf{T}_M : \operatorname{grad} \mathbf{x}_M' - (\mathbf{T}_M - \breve{\mathbf{S}}_M) : \bar{\boldsymbol{\nu}}_M + \breve{\mathbf{Q}}_M^3 \, \vdots \, \operatorname{grad} \bar{\boldsymbol{\nu}}_M, \tag{4}$$

$$\rho_0 \, \varepsilon_M' \; = \; \mathbf{P}_M : \operatorname{GRAD} \mathbf{x}_M' - \left((\mathbf{P}_M - \mathbf{S}_M) \cdot \mathbf{F}_M^T \right) : \bar{\boldsymbol{\nu}}_M + \mathbf{Q}_M^3 \, \vdots \, \operatorname{GRAD} \bar{\boldsymbol{\nu}}_M, \tag{5}$$

respectively. Eq. (5) can be resorted and we may write

$$\rho_0 \, \varepsilon_M' \; = \; \bar{\mathbf{P}}_M : \operatorname{GRAD} \mathbf{x}_M' + \bar{\mathbf{Q}}_M^3 \, \vdots \, \operatorname{GRAD} \bar{\boldsymbol{\chi}}_M' + \bar{\mathbf{S}}_M : \left(\overset{*}{\boldsymbol{\chi}}_M \right)', \tag{6}$$

where

$$\overset{*}{\boldsymbol{\chi}}_M \; = \; \bar{\boldsymbol{\chi}}_M - \mathbf{F}_M, \tag{7}$$

$$\bar{\mathbf{P}}_M \; = \; \mathbf{P}_M + \bar{\mathbf{S}}_M, \tag{8}$$

$$\bar{\mathbf{S}}_M \; = \; (\mathbf{S}_M - \mathbf{P}_M) \cdot \mathbf{F}_M^T \cdot \bar{\boldsymbol{\chi}}_M^{T-1} \; \text{and} \tag{9}$$

$$\bar{\mathbf{Q}}_M^3 \; = \; \mathbf{Q}_M^3 \, \hat{:} \, \left(\bar{\boldsymbol{\chi}}_M^{T-1}, \mathbf{I} \right). \tag{10}$$

Note that the expression $\overset{*}{\boldsymbol{\chi}}_M$ is achieved only by a rearrangement of eq. (5). For the small deformation regime, $\overset{*}{\boldsymbol{\chi}}_M$ describes the difference between the micro- and the macrodeformation. However, this physical interpretation does not hold for the finite deformation regime, where the difference between the micro- and the macrofield takes the form $\bar{\boldsymbol{\chi}}_M^{-1} \cdot \mathbf{F}_M$, cf. Eringen (1999); Jänicke et al. (2009). In that case, $\overset{*}{\boldsymbol{\chi}}_M$ only covers a formal evidence without a direct physical interpretation.

2.3 Scale transition of the kinematic quantities

In order to characterise materials with strong inhomogeneities on the microscale, it is our intend to introduce a consistent averaging technique replacing the heterogeneous Cauchy medium by a homogeneous micromorphic medium. An appropriate methodology has been initially proposed by Forest and Sab (1998); Forest (1999). Moreover, it has been presented in detail by Jänicke et al. (2009). Thus, the kinematic quantities of the micromorphic macrocontinuum can be identified in terms of a polynomial mean field and a periodic fluctuation of the heterogeneous Cauchy microcontinuum attached to the micromorphic material point. To simplify matters, we assume the attached microvolume to be a quadratic unit cell of the size l as depicted in fig. 2. Furthermore, we assume the set $(\mathbf{u}_M, \bar{\boldsymbol{\chi}}_M)$ to characterise the macrostate that best fits the microscopic displacement field $\mathbf{u}_m$ in the average over the attached microvolume. For the sake of simplicity, the following investigations are restricted for the twodimensional case.
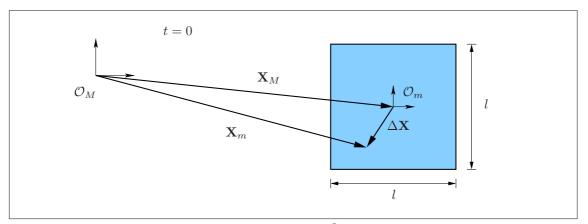
Figure 2. The 2-D microscopic volume element of the size l^2 attached to the macroscopic material point. Its volume centroid is defined by the macroscopic position vector $\mathbf{X}_M$, the local coordinate is indicated by the so-called branch vector $\Delta\mathbf{X}$ (material frame, t=0).

I. e. we have to minimise the functional

$$\mathcal{F}(\mathbf{u}_M, \bar{\boldsymbol{\chi}}_M) = \left\langle (\mathbf{u}_m - \mathbf{u}_M - (\bar{\boldsymbol{\chi}}_M - \mathbf{I}) \cdot \Delta\mathbf{X})^2 \right\rangle \tag{11}$$

with the volume average $\langle \diamond \rangle = 1/V_m \int_{\mathcal{B}_m} \diamond \, dV_m$. We find

$$\Delta\mathbf{u} = \mathbf{u}_m - \mathbf{u}_M = \mathbf{0} \text{ and } \bar{\boldsymbol{\chi}}_M - \mathbf{I} = \frac{12}{l^2} \langle \mathbf{u}_m \otimes \Delta\mathbf{X} \rangle \tag{12}$$

for the local displacements and for the micromotion, respectively. Consequently, the particular gradients read

$$\text{GRAD}\,\mathbf{u}_M = \langle \text{GRAD}\,\mathbf{u}_m \rangle \text{ and } \text{GRAD}\,\bar{\boldsymbol{\chi}}_M = \frac{12}{l^2} \langle \text{GRAD}\,(\mathbf{u}_m \otimes \Delta\mathbf{X}) \rangle. \tag{13}$$

If we furthermore assume the microscopic displacement field to be a polynomial of grade three, we may express the microscopic displacement field $\Delta\mathbf{u}$ in terms of the macroscopic deformation quantities and we obtain

$$\Delta\mathbf{u} = \text{GRAD}\,\mathbf{u}_M \cdot \Delta\mathbf{X} + \frac{1}{2}\text{GRAD}\,\bar{\boldsymbol{\chi}}_M : (\Delta\mathbf{X} \otimes \Delta\mathbf{X})$$

$$- \frac{10}{l^2} \overset{*}{\boldsymbol{\chi}}_M \cdot \overset{4}{\mathbf{E}} \vdots (\Delta\mathbf{X} \otimes \Delta\mathbf{X} \otimes \Delta\mathbf{X}) + \Delta\tilde{\mathbf{u}}. \tag{14}$$

Whereas the linear deformation modes are dominated by the macroscopic displacement gradient, the quadratic deformation modes depend on the gradient of the microdeformation $\text{GRAD}\,\bar{\boldsymbol{\chi}}_M$, the cubic deformation modes on the difference deformation $\overset{*}{\boldsymbol{\chi}}_M = \bar{\boldsymbol{\chi}}_M - \mathbf{F}_M$. $\Delta\tilde{\mathbf{u}}$ represents a fluctuation field due to the microstructural periodicity. Having in mind the linear displacement field $\Delta\tilde{\mathbf{u}} = \text{GRAD}\,\mathbf{u}_M \cdot \Delta\mathbf{X} + \Delta\tilde{\mathbf{u}}$ of a so-called first-order FE^2 approach replacing a heterogeneous Cauchy microcontinuum by a homogeneous Cauchy macrocontinuum, e. g. Feyel and Chaboche (2000); Miehe and Koch (2002); Sehlhorst et al. (2009), eq. (14) is pointing out the extended character of the introduced projection rule.

Special attention should be paid to the interaction between the higher order deformation modes and the size of the attached microvolume. Let us rewrite eq. (14) in a dimensionless manner,

$$\frac{\Delta\mathbf{u}}{l} = \text{GRAD}\,\mathbf{u}_M \cdot \frac{\Delta\mathbf{X}}{l} + \frac{1}{2}\boxed{l\,\text{GRAD}\,\bar{\boldsymbol{\chi}}_M} : \left(\frac{\Delta\mathbf{X}}{l} \otimes \frac{\Delta\mathbf{X}}{l}\right)$$

$$- 10\,\overset{*}{\boldsymbol{\chi}}_M \cdot \overset{4}{\mathbf{E}} \vdots \left(\frac{\Delta\mathbf{X}}{l} \otimes \frac{\Delta\mathbf{X}}{l} \otimes \frac{\Delta\mathbf{X}}{l}\right) + \frac{\Delta\tilde{\mathbf{u}}}{l}. \tag{15}$$

Thus, we find the quadratic polynomial expansion to transport the size of the microvolume from the micro- to the macroscale by the expression $l\,\text{GRAD}\,\bar{\boldsymbol{\chi}}_M$. Comparable results have been found e. g. by Kouznetsova (2002); Larsson and Diebels (2006); Jänicke and Diebels (2009). By contrast, the cubic expansion has, per division by l^2, a size-independent character which enriches the linear deformation modes and allows the system to describe more complex but size-independent deformation mechanisms.

The projection rules eqs. (14) and (15), respectively, can be specified for any micromorphic subcontinuum with any restricted microdeformation, e. g. micropolar, microdilatant or microshear deformation, cf. Forest (2006); Jänicke et al. (2009).

2.4 Hill-Mandel condition and homogenisation of stresses

After having derived appropriate projection rules defining a Dirichlet boundary value problem at the boundary of the heterogeneous microvolume in terms of the extended macrodeformations, we now have to find a connection between the stress response of the Cauchy microcontinuum and the stresses, couplestresses and hyperstresses of the micromorphic macrocontinuum. The fundamental assumption to deduce the homogenisation rules is the equivalence of the strain energy rate in the macroscopic material point and of the volume average of the microscopic strain energy rate of the attached microvolume. This correlation is commonly called Hill-Mandel condition, cf. Hill (1963); Maugin (1992); Nemat-Nasser and Hori (1993). Thus, we may write

$$\langle \mathbf{P}_m : \text{GRAD}\,\Delta\mathbf{u}' \rangle = \bar{\mathbf{P}}_M : \text{GRAD}\,\mathbf{u}'_M + \bar{\mathbf{Q}}^3_M \stackrel{.}{:} \text{GRAD}\,\bar{\chi}'_M + \bar{\mathbf{S}}_M : \left(\stackrel{*}{\chi}_M\right)'. \tag{16}$$

Inserting eq. (14) in eq. (16) leads to the expressions

$$\bar{\mathbf{P}}_M = \frac{1}{V_m} \int_{\partial \mathcal{B}_m} (\mathbf{p}_m \otimes \Delta\mathbf{X})\,\mathrm{d}A, \tag{17}$$

$$\bar{\mathbf{Q}}^3_M = \frac{1}{2\,V_m} \int_{\partial \mathcal{B}_m} (\mathbf{p}_m \otimes \Delta\mathbf{X} \otimes \Delta\mathbf{X})\,\mathrm{d}A, \tag{18}$$

$$\bar{\mathbf{S}}^4_M = \frac{1}{6\,V_m} \int_{\partial \mathcal{B}_m} (\mathbf{p}_m \otimes \Delta\mathbf{X} \otimes \Delta\mathbf{X} \otimes \Delta\mathbf{X})\,\mathrm{d}A, \tag{19}$$

where $\mathbf{p}_m$ represents the microscopic surface traction vector. Concerning the periodic fluctuations $\Delta\tilde{\mathbf{u}}$, one may establish opposite parts of the microvolume's boundary $\partial \mathcal{B}^+_m$ and $\partial \mathcal{B}^-_m$ in a way that the correlation $\mathbf{N}^+ = -\mathbf{N}^-$ is satisfied for the outer normal vectors of corresponding points on $\partial \mathcal{B}^+_m$ and $\partial \mathcal{B}^-_m$. Provided the existence of periodic displacements and anti-periodic tractions on opposite parts of the boundary, i. e.

$$\Delta\tilde{\mathbf{u}}^+ = \Delta\tilde{\mathbf{u}}^- \quad \text{and} \quad \mathbf{p}^+_m = -\mathbf{p}^-_m, \tag{20}$$

the periodic fluctuations do not account for the strain energy. Furthermore, the fourth order hyperstress tensor $\bar{\mathbf{S}}^4_M$ resulting from the homogenisation procedure has to be transferred back to a second order quantity via the identity

$$\bar{\mathbf{S}}^2_M = -\frac{60}{l^2}\,\bar{\mathbf{S}}^4_M \stackrel{4}{:} \stackrel{4}{\mathbf{E}} \tag{21}$$

making use of eqs. (14) and (16).

3 Microscopic deformation mechanisms of a periodic model-foam

After having completed the numerical homogenisation procedure in the sections before, we now want to implement this second order FE^2 scheme. For that purpose, we introduce a perfectly periodic structure in 2-D with a cross-like unit cell of the size l^2, representing the attached microvolume within the two-scale approach, cf. fig. 3a. The microscale is resolved by quadrilateral volume elements with biquartic Lagrange Ansatz functions. We assume linear elasticity in a small deformation regime with Young's modulus $Y = 200\,\text{GPa}$ and Poisson's ratio $\nu = 0.33$. For the microscale calculations, periodic boundary conditions have been applied. In doing so, the fluctuations $\Delta\tilde{\mathbf{u}}$ have been suppressed at the midpoints of every strut on the boundary.

On the macroscale, a numerical shear test of an infinitely long domain with variable thickness h has been carried out. The experimental setup is depicted in fig. 3b. Besides the Dirichlet boundary conditions for the displacements, the microdeformation on the top and the bottom boundary has been restricted to equal the identity. The macrolevel has been resolved by quadrilateral volume elements with biquadratic Lagrange Ansatz functions for both, the displacement and the microdeformation field.
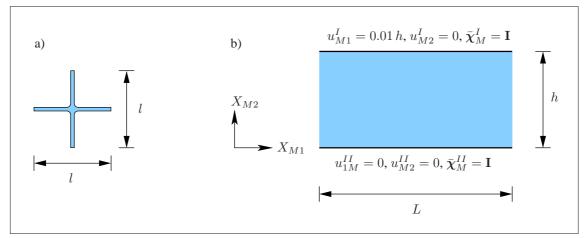
Figure 3. a) The underlying, perfectly periodic microvolume of the size $l = 20\,d$. Linear elasticity in a small deformation regime is assumed (Young's modulus $Y = 200\,\text{GPa}$, Poisson's ratio $\nu = 0.33$). The struts are resolved by quadrilateral volume elements with quartic Lagrange Ansatz functions. b) The experimental setup on the macroscale describes a shear test of an infinite layer ($L \to \infty$) of the variable thickness $h > l$. At both, the top and the bottom boundary, the extended degrees of freedom are prescribed to vanish, i. e. the microdeformation tensor equals the identity $\bar{\boldsymbol{\chi}}_M = \mathbf{I}$.

Having in mind the restriction of the full micromorphic continuum to a micromorphic subcontinuum mentioned in section 2.3, the question arises, if there is any reasonable restriction of the microdeformation subject to the given microstructure, cf. fig. 3a. For that purpose, the quadratic deformation modes in dependence of $\bar{\chi}_{M12}$ and $\bar{\chi}_{M21}$ have been depicted in figs. 4 and 5 as well as their symmetric and skew-symmetric counterparts. Due to the macroscopic geometry given in fig. 3b, only derivatives in X_{M2}-direction have been taken into account.

The deformation states depicted in figs. 4 and 5 clearly indicate the skew-symmetric microdeformation $\bar{\chi}_{M12} = -\bar{\chi}_{M21}$ to be the most natural choice which leads to the well-known micropolar continuum or Cosserat continuum, respectively. For the small deformation regime, we may write

$$\bar{\chi}_{M11} = \bar{\chi}_{M22} = 1 \quad \text{and} \quad -\bar{\chi}_{M12} = \bar{\chi}_{M21} = \bar{\varphi}_M. \tag{22}$$

It is the main issue of the following section to verify the found indication for a micropolar or Cosserat continuum.
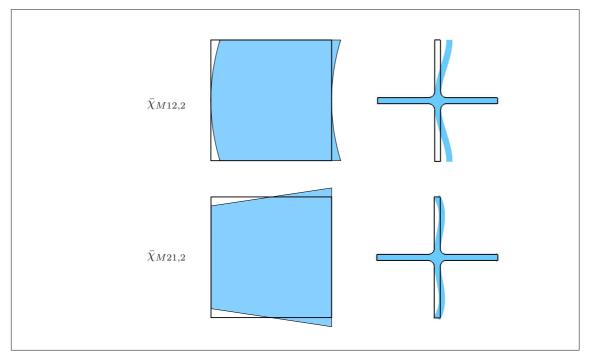

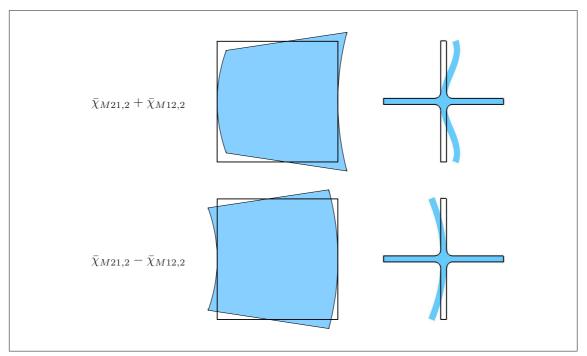Figure 4. Several characteristic quadratic deformation modes.

Figure 5. Several characteristic quadratic deformation modes.

4 Two-scale calculation

To do so, we have accomplished several FE^2 calculations of the above mentioned shear test, i. e., for the macroscale, using a Cosserat continuum on the one hand, compared to the application of a full micromorphic continuum on the other hand. To furthermore demonstrate the difference between the extended homogenisation scheme and a first order approach, a third FE^2 calculation deals with a Cauchy continuum on the macroscale. Finally, to evaluate the found results in a quantitative way, a reference calculation has been carried out, where the entire microstructure of the macroscopic boundary value problem, cf. fig. 3b, has been microscopically resolved by finite elements, i. e. without making use of any FE^2 methodology. The results are given in fig. 6.
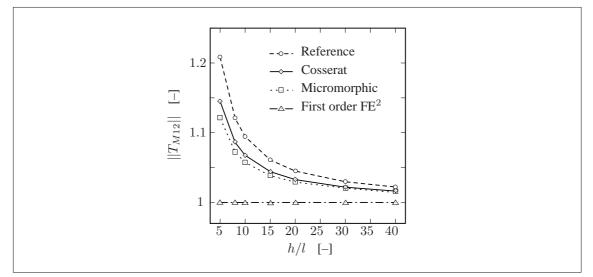

Figure 6. Effective shear stress $||T_{M12}||$, normalised with respect to the constant result of the first order FE^2 solution, over the ratio h/l.

At first, we find the reference solution to describe an increasing effective shear stress with a decreasing ratio h/l, i. e. the material features the well-known stiff boundary-layer effect, e. g. beyond many others Diebels and Steeb (2002); Tekoğlu and Onck (2008). Thus, the effective shear stress of the reference solution is about 17% higher for $h/l = 5$ than it is for $h/l = 40$. Furthermore, one may determine the effective shear stress to converge for large sample sizes, i. e. the stiffening effect of the boundary layers becomes less pronounced if the sample size increases

for a fixed microstructure. If we now consider the first order FE^2 solution, we find that, as expected, the solution does not behave sensitive for the stiff boundary layer. This is due to the lack of higher order deformations, especially bending modes, which dominate the deformation close to the boundary. But, obviously both, the reference and the first order FE^2 solution, seem to converge towards the same value for large sample sizes h.

By contrast, the Cosserat solution and, only in a slightly weaker way, the micromorphic solution, are able to reproduce the bending effects quite well. But we still observe a certain difference between the reference and the second order FE^2 solutions. E. g. for $h/l = 10$, the effective shear stress of the micromorphic calculation is about 3% weaker than the reference value. One possible explanation for this slight difference could be found in the choice of the microscopic Dirichlet and periodic boundary conditions, which may be chosen too weak. Furthermore, we observe the micromorphic solution to be weaker than the Cosserat solution. This effect can be interpreted as a consequence of the less restricted character of the full micromorphic medium, which allows for deformation modes not included in the Cosserat theory. By consequence, the Cosserat solution only pretends to result in a more exact result than the micromorphic solution. But, obviously, this effect is very small and may be neglected in our case.

To illustrate the increasing influence of the stiff boundary layer with decreasing macroscopic sample size, the microrotation $\bar{\varphi}_M$ has been plotted over the normalised macroscopic sample height for different ratios h/l in fig. 7.
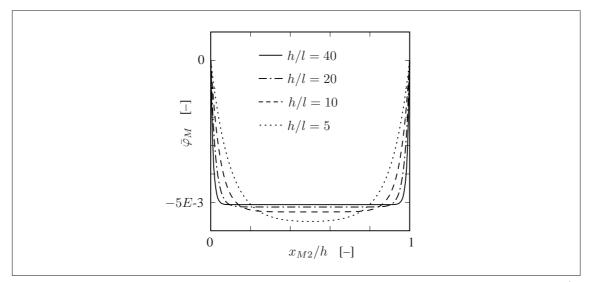

Figure 7. Microrotation $\bar{\varphi}_M = -\bar{\chi}_{M12} = \bar{\chi}_{M21}$ for the Cosserat calculation for different sample sizes h/l over the normalised height of the sample.

Finally, we want to point out the higher order deformation modes to be meaningful from the physical point of view. Thus, in fig. 8, two representative microscopic deformation states are depicted. To do so, the macroscopic deformation measures have been evaluated for the micromorphic FE^2 solution (sample size $h = 20\,l$) at the positions $X_{M2} = 10\,l$ and $X_{M2} = 20\,l$. Afterwards, they have been projected back to the boundary of the attached microvolume in order to find the given visualisation. Considering fig. 8a, i. e. the situation far away from the boundary, we find the microvolume under shear without any bending deformation. Obviously, the situation changes completely if we reach the boundary. Here, the bending supersede the shear effects, cf. fig. 8b.
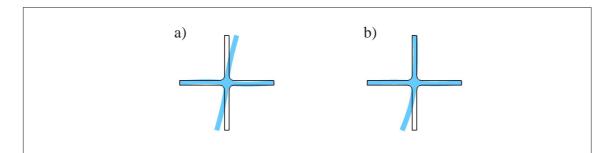
Figure 8. Two representative microscopic deformation states observed in the micromorphic FE^2 solution for the macroscopic sample size $h = 20\,l$ at the positions a) $X_{M2} = 10\,l$ and b) $X_{M2} = 20\,l$. To generate the above plots, the macroscopic deformation quantities have been reprojected to the microscale using eq. (14).

5 Conclusions and ongoing work

To summarise the present study, we want to highlight again the found results in a clearly arranged manner:

- It has been shown the higher order numerical homogenisation approach, dealing with a micromorphic continuum theory on the macroscale, to be able to describe the stiff boundary layer effect under shear deformation for a given microstructure. This is not possible applying a first order approach.

- A quantitative comparison to a reference calculation with microscopical resolution has been accomplished. The small but measurable difference in the effective shear stress may be explained by the special choice of boundary conditions on the microlevel.

- By studying the deformation mechanisms of the proposed microstructure, it has been possible to restrict the micromorphic macrocontinuum to undergo skew-symmetric microdeformations, i. e. to be of the micropolar or Cosserat type, respectively. The results of the FE^2 calculations support that assumption.

Doubtless, a general disadvantage of any FE^2 calculation might be that it requires a certain numerical effort, especially if carried out for finite deformations, nonlinear material behaviour and for less regular microstructures. But otherwise, a purely macroscopic extended continuum model supposes the identification of extended material parameters which are, in general, hard to find in physical experiments. Applying the higher-order homogenisation approach, the macroscopic constitutive modelling is shifted to the well-defined microlevel. The definition of any extended material parameter is a priori circumvented. Thus, the proposed homogenisation methodology seems to be a helpful tool to describe microtopologically-driven higher order effects and it may help to achieve a deeper understanding of the interaction between microscopic processes and the effective macroscopic material behaviour.

In the future, further efforts have to be carried out to explore the influence of the microscopic boundary conditions on the effective macroscopic stress response. Furthermore, the present study has to be extended to a various set of more complex microstructures in different macroscopic loading cases. Thereby, special attention has to be paid to the general limits of the proposed mean-field theory, if the microstructure exhibits stochastic irregularities and imperfections (micro-fractures, cavities, dislocations etc.)

References

Cosserat, E.; Cosserat, F.: *Théorie des corps déformables*. A. Hermann et Fils, Paris (1909).

Diebels, S.; Steeb, H.: The size effect in foams and its theoretical and numerical investigation. *Proc. R. Soc. Lond. A*, 458, (2002), 2869–2883.

Eringen, C.: *Microcontinuum Field Theories, Vol. I: Foundations and Solids*. Springer-Verlag, Berlin (1999).

Feyel, F.; Chaboche, J. L.: FE^2 multiscale approach for modelling the elastoviscoplastic behaviour of long fiber SiC/Ti composite materials. *Comp. Meth. Appl. Mech. Eng.*, 183, (2000), 309–330.

Forest, S.: Homogenization methods and the mechanics of generalized continua. In: G. Maugin, ed., *Geometry, Continua and Microstructure*, Travaux en Cours, No. 60, pages 35–48, Hermann, Paris (1999).

Forest, S.: Nonlinear microstrain theories. *Int. J. Solids Structures*, 43, (2006), 7224–7245.

Forest, S.; Sab, K.: Cosserat overall modeling of heterogeneous materials. *Mech. Res. Commun.*, 25, (1998), 449–454.

Germain, P.: La méthode des puissances virtuelles en mécanique des milieux continus, Première partie: Théorie du second gradient. *J. Mecanique*, 12, (1973a), 235–274.

Germain, P.: The method of virtual power in continuum mechanics. Part 2: Microstructure. *SIAM J. Appl. Math.*, 25, (1973b), 556–575.

Hill, R.: Elastic properties of reinforced solids: Some theoretical principles. *J. Mech. Phys. Solids*, 11, (1963), 357–372.

Jänicke, R.; Diebels, S.: A numerical homogenisation strategy for micromorphic continua. *Nuovo Cimento Soc. Ital. Fis. C*, 31 (1), (2009), 121–132.

Jänicke, R.; Diebels, S.; Sehlhorst, H. G.; Düster, A.: Two-scale modelling of micromorphic continua. *Continuum Mech. Therm.*, DOI 10.1007/s00161-003-0114-4.

Kouznetsova, V. G.: *Computational homogenization for the multi-scale analysis of multi-phase materials*. PhD-thesis, Technische Universiteit Eindhoven, The Netherlands (2002).

Larsson, R.; Diebels, S.: A second order homogenization procedure for multi-scale analysis based on micropolar kinematics. *Int. J. Numer. Meth. Eng.*, 69, (2006), 2485–2512.

Maugin, G. A.: Nonlocal theories or gradient-type theories: A matter of convenience? *Acta Mater.*, 31, (1979), 15–26.

Maugin, G. A.: *The Thermomechanics of Plasticity and Fracture*. Cambridge University Press, Cambridge (1992).

Miehe, C.; Koch, A.: Computational micro-to-macro transitions of discretized microstructures undergoing small strains. *Arch. Appl. Mech.*, 72, (2002), 300–317.

Nemat-Nasser, S.; Hori, M.: *Micromechanics*. North-Holland, Amsterdam (1993).

Sehlhorst, H.-G.; Jänicke, R.; Düster, A.; Rank, E.; Steeb, H.; Diebels, S.: Numerical investigations of foam-like materials by nested high-order finite element methods. *Comp. Mech.*, 45(1), (2009), 45–59.

Tekoğlu, C.; Onck, P. R.: Size effects in the mechanical behaviour of cellular materials. *J. Mat. Sci.*, 40, (2005), 5911–3564.

Tekoğlu, C.; Onck, P. R.: Size effects in two-dimensional voronoi foams: A comparison between generalized continua and discrete models. *J. Mech. Phys. Solids*, 56, (2008), 3541–3564.

Address: Ralf Jänicke and Stefan Diebels,
Lehrstuhl für Technische Mechanik, Universität des Saarlandes, Campus A4 2, 66123 Saarbrücken
email: r.jaenicke@mx.uni-saarland.de; s.diebels@mx.uni-saarland.de